Title

Accuracy of omni-planar and surface casting of epileptiform activity for intracranial seizure localization

Journal

Epilepsia, 62(4)

ISSN

0013-9580

Authors

Kleen, Jonathan K
Speidel, Benjamin A
Baud, Maxime O
et al.

Publication Date

2021-04-01

DOI

10.1111/epi.16841

Peer reviewed

HHS Public Access

Author manuscript

Epilepsia. Author manuscript; available in PMC 2021 July 13.

Published in final edited form as:

Epilepsia. 2021 April ; 62(4): 947–959. doi:10.1111/epi.16841.

Accuracy of omni-planar and surface casting of epileptiform activity for intracranial seizure localization

Jonathan K. Kleen[1], **Benjamin Speidel**[1], **Maxime O. Baud**[2], **Vikram R. Rao**[1], **Simon G. Ammanuel**[1], **Liberty S. Hamilton**[3], **Edward F. Chang**[4], **Robert C. Knowlton**[1]

[1]Department of Neurology and Weill Institute for Neurosciences, University of California, San Francisco [2]Department of Neurology, Inselspital, University Hospital Bern, University of Bern, Bern, Switzerland [3]Department of Speech, Language, and Hearing Sciences and Department of Neurology, The University of Texas at Austin [4]Department of Neurological Surgery and Weill Institute for Neurosciences, University of California, San Francisco

SUMMARY

Objective: Intracranial electroencephalography (ICEEG) recordings are performed for seizure localization in medically-refractory epilepsy. Signal quantifications such as frequency power can be projected as heatmaps on personalized 3D reconstructed cortical surfaces to distill these complex recordings into intuitive cinematic visualizations. However, simultaneously reconciling deep recording locations and reliably tracking evolving ictal patterns remain significant challenges.

Methods: We fused oblique MRI slices along depth probe trajectories with cortical surface reconstructions and projected dynamic heatmaps using a simple mathematical metric of epileptiform activity (line-length). This omni-planar and surface casting of epileptiform activity approach (OPSCEA) thus illustrated seizure onset and spread among both deep and superficial locations simultaneously with minimal need for signal processing supervision. We utilized the approach on 41 patients at our center implanted with grid, strip, and/or depth electrodes for localizing medically-refractory seizures. Peri-ictal data was converted into OPSCEA videos with multiple 3D brain views illustrating all electrode locations. Five people of varying expertise in epilepsy (medical student through epilepsy attending level) attempted to localize the seizure-onset zones.

Correspondence to: Edward.Chang@ucsf.edu and Robert.Knowlton@ucsf.edu, 400 Parnassus Avenue, 8th Fl., San Francisco, CA 94143 USA, Phone: 415-353-2437, Fax: 415-353-2837.

Data and code accessibility: The Matlab-based code used to reproduce the demonstrated cases (Figures 2, 3, 4) is available on GitHub (http://github.com/Kleen-Lab) along with links to the other relevant software packages used herein. The high resolution video versions for these cases (Videos 1, 2, 3, 4) are available on YouTube (https://www.youtube.com/playlist?list=PLGmfrsRwdva-WKwqLyWwcZxE0f_MA9vIL). The de-identified sample datasets to make practice videos are available for download on Open Source Framework (https://osf.io/49znp/).

Disclosure of conflicts of interest:
None of the authors has any conflict of interest to disclose.

Ethical publication statement: We confirm that we have read the Journal's position on issues involved in ethical publication and affirm that this report is consistent with those guidelines.

Results: We retrospectively compared this approach with the original ICEEG study reports for validation. Accuracy ranged from 73.2 to 97.6% for complete or overlapping onset lobe(s) respectively, and approximately 56.1 to 95.1% for the specific focus (or foci). Higher answer certainty for a given case predicted better accuracy, and scorers had similar accuracy across different training levels.

Significance: In an era of increasing stereo-EEG use, cinematic visualizations fusing omni-planar and surface functional projections appear to provide a useful adjunct for interpreting complex intracranial recordings and subsequent surgery planning.

Keywords

Epilepsy; Electrocorticography (ECoG); Stereo-EEG; Visualization; Propagation

INTRODUCTION

Intracranial EEG (ICEEG) recordings provide unparalleled perspectives for direct seizure localization in humans. Certain patients with medically-refractory focal epilepsy undergo these recordings in the hope that implanted electrodes will encounter the seizure onset zone(s) or network (SOZ) and provide a topographical resection guide for the neurological surgeon and/or aid in neurostimulator implantation planning. The precise localization of the SOZ during ICEEG recordings is key to surgical success. While improved diagnostics may yield improved surgical outcomes(1), the deluge of data deepens as ICEEG recordings become more complex and scale to higher densities(2).

While scalp EEG electrode placement is standardized (i.e. 10-20 or 10-10 systems), ICEEG requires the clinically-directed placement of up to hundreds of electrodes in locations unique to each patient, often including several depth probes(3). Tailored implantations are necessary to account for pre-surgical localization clues including semiology, imaging findings, and anatomical constraints (e.g. major vessels to avoid). These and many other factors vary across patients (Table 1). The epileptologist must become accustomed to the unique layout of the EEG traces and unite this with a mental map of their anatomic origins. Finally, locations must be reaffirmed frequently as new phenomena and seizures arise during the long-term recording, and these challenges recur in full when communicating to clinical team members.

Personalized brain reconstructions provide more natural visualization of patient-specific anatomy and implanted electrode locations(4-6). Neural activity can then be colorized on these surfaces (heatmaps) to comprehend functional topography, akin to methods commonly employed in other imaging modalities, such as functional MRI, ictal single photon emission computed tomography, and magnetoencephalography(7-9).

Such methods have also been used to localize seizures from ICEEG using specific oscillation power bands as ictal activity indices(6,10-12) including within open-source platforms(13,14). However, fixed frequency parameters pose limitations since ictal frequency admixtures often evolve quickly and range from delta to pathologically fast high gamma frequencies (>200 Hz). Also, despite the rising ubiquity of stereo-EEG (SEEG)

approaches relying solely on depth electrodes(3,15), previous reports(6,10) similar to our proposed “cinematic” approach here utilized only cortical surface views, largely obscuring deep structure activity.

Here we first show that co-registered MRI volume slices along depth probe trajectories at any angle (omni-planar) provide additional intuitive and anatomically-accurate ictal projection surfaces (“digitally *in situ*”). We then apply a simplified signal transformation (line-length) that incorporates broadband information while being sensitive to epileptiform features(16-18) requiring minimal supervision. We refer to this approach as Omni-Planar and Surface Casting of Epileptiform Activity (OPSCEA, referencing the homonym Greek suffix -*opsia* as in sight or visual inspection). Toward clinical validation, we asked a panel of scorers from a range of clinical expertise levels to identify the SOZ using the OPSCEA method and compared their results to the clinical reference standard (CRS; the original clinically-determined SOZ by expert epileptologists using trace-based ICEEG review as verified by retrospective chart review).

MATERIALS AND METHODS

Subjects

This study included 41 patients with medically-refractory focal seizures who underwent intracranial implantation of grid, strip, and/or depth electrodes for pre-surgical seizure localization (Table S1). These patients were selected to represent a diverse mix of SOZs and spread patterns, including cortical surface and deep locations. Patients gave their written informed consent and the research protocol was approved by the UCSF Committee on Human Research. For each patient, an expert attending epileptologist (RCK, non-scorer) selected up to six seizure examples for OPSCEA videos based on their direct influence on the CRS, and confirmed whether the CRS itself had been considered well-localized or not (Table S1).

ICEEG recordings and signal processing

Recordings were preprocessed by first low-pass filtering (< 255 Hz), then downsampling (from 1024-3052 Hz) to 512 Hz. Channels with artifact or which otherwise were not recording neural signal (e.g. outside the brain) were removed from the analysis, and notch filters were applied (60Hz and harmonics). For recordings affected by movement or other artifact affecting all channels a common average reference was applied to the entire recording (mean, or median if focal large-amplitude discharges were present around the time of seizure onset(19)).

The ICEEG data was then transformed using line-length (LL; Figure S1), which is the sum of absolute differences between consecutive samples of an ICEEG segment for a given window of data(16). LL has good sensitivity and specificity as a metric of epileptiform activity (for example it is frequently used as the detection setting in responsive neurostimulators)(16,18). We used default transform windows of 500 ms, but opted for longer one-second windows for certain patients with slow rhythmic ictal discharges (e.g. 0.5-1.0 Hz) since we found that ensuring an overlap of at least one full period of this

discharge rhythmicity provides more stable heatmaps during video playback. Conversely we titrated much shorter windows (50, 100, or 250 ms) for patients with sudden widespread ictal onsets or rapid burst propagation patterns, with the window duration guided by the approximate amount of time for >50% of channels to be involved in the ictal onset or propagating burst (see Results). LL was calculated in point-by-point sliding fashion, enabling video frame time resolution down to the original (or downsampled) sampling frequency if desired. We then normalized LL for each channel to a pre-ictal baseline (a 10 second period free of epileptiform features, or shorter duration if required due to spike burden), converting LL to a pre-ictal-based z-score quantity (zLL). We found this to be a crucial step that adjusted for inter-electrode differences.

Functional projection: Surfaces

Each participant underwent a pre-operative MRI and post-operative CT for co-registration of electrode locations. MRI T1 series voxel data was reformatted and channeled through our in-house research pipeline img_pipe(4), combined with FreeSurfer(5) (Charlestown, MA) for detailed cortical surface renderings of each hemisphere, though any surface rendering package is feasible(6). The coordinates of co-registered electrodes were then plotted into the same 3D digital space (Figure 1D). Similar to prior methods for cortical surface projection(6,10) we colorized the nearby surface mesh (Figure 1D, right panel) according to ictal signal intensity and the distances of the anatomical surfaces to an electrode. While previous work(10) assumed a linear drop-off, signal intensity falls inversely proportional to squared distance(20), therefore we opted for a Gaussian spreading parameter as an intermediate drop-off function for electrode weights(4). Values were interpolated across the surface using this function and normal-vector interpolation shading using the MATLAB *interp* and *phong* functions.

Functional projection: Omni-planar slices

We then sought to reveal depth electrode activity using the same color scale projected onto 2D slices of the 3D MRI voxel data. However, cardinal planes (coronal, sagittal, horizontal) are rarely in precise alignment with depth electrodes since exact orthogonal or parasagittal placements are infrequent due to clinical needs and anatomic constraints (15,21,22).

To solve this issue, we calculated the yaw-axis (horizontal plane) trajectory for each depth electrode using the angle cosine of the flanking (innermost and outermost) electrodes. Here, X and Y correspond to medial-lateral and anterior-posterior dimensions. From this trajectory we then defined a 2D plane that ran exactly parallel to the depth electrode trajectory and extended vertically in the superior-inferior (Z) axis. We then captured all brain tissue voxels intersecting this 2D plane. This resulting 2D image (voxels converted to pixels; Figure 1E) was plotted as an additional surface and co-registered in 3D space, enabling the same functional projection steps upon accurate anatomy surrounding each depth electrode. As a final step, the portion of cortical surface positioned between the viewer (“camera”) and the 2D slice was removed, creating a “lopped off” appearance (Figure 1E right panel; Figure S2). Similar to the surface renderings, these omni-planar reconstructions are thus anatomically personalized to the patient (grey and white matter organization, lesion details, etc).

Multi-view cinematic rendering

Peri-ictal ICEEG recordings were converted into videos with multiple views of the available coverage to assist simultaneous assessment. Default views included lateral and inferior cortical surface views and an omni-planar slice view for each individual depth electrode. For the latter, all other depth probe electrodes were omitted from a given depth's omni-planar heatmap rendering for clarity since they were rarely in-plane. Additional angles were added or removed for a given patient ensuring activity from every electrode site could be visualized. As a reference for depth probe trajectories, color-coded lines traversing the horizontal plane were shown in an inferior view of a semi-transparent ("glass") brain in a separate panel. An example patient is shown in Figure 2 (also see Video S1) with frontal, parietal, temporal (lateral and basal) grid and strip coverage, along with depth electrodes in the hippocampus, amygdala, insula, and cingulate gyrus.

ICEEG tracings were displayed adjacent to the videos for timing and comparison purposes (though see blinding procedure below), with a gray window outlining the data projected in each frame (Figure 2B). Each patient's customized composite view of subplots was typecast for all of their seizure videos since implantation coverage did not change. For computational efficiency and code reproducibility across patients, these composite views were produced from a standardized matrix itemizing parameter details for each subplot.

Temporal resolution is flexible though higher frame rates increase video-rendering time and video file sizes. For computational efficiency, and since most seizures do not require high temporal resolution to see onset and spread, we often defaulted to 4 frames per second of data (FPSD) and a 50% overlapping window at minimum (see above regarding transform window durations). For finer spatiotemporal detail of rapidly propagating activity, we used a FPSD of 30 or more to ensure the spatiotemporal extent of a rapidly propagating burst could be observed across at least 10 frames. Video playback speed (PBS) was defaulted to 15 frames per second. Therefore, for example, if the user desired 5 frames per second of data, the video would play at triple real-time speed (PBS/FPSD = 15/5 = 3).

Video scoring participants and procedure

There were 5 video scorers across of diverse training levels: one board-certified epileptologist, one epilepsy fellow, two residents (neurology, neurosurgery), and one senior medical student. All gave written informed consent to be a subject for this research and this portion was also approved by the UCSF Committee on Human Research. These individuals independently viewed seizure video(s) for each of the 41 patients and could replay frame-by-frame if desired. The ICEEG tracings were also shown at right, but since overt ictal activity on traces could bias scorers, for blinding purposes the channel order was randomized and channel labels were removed.

Participants were asked to approximate where each patient's seizures start by providing the name(s) of a neuroanatomic region such as the specific gyrus, deep structure, or larger region, such as a lobe if more appropriate. They also circled or drew arrows on a screenshot printout of each patient's video for added scoring certainty, and scorers were also asked to rate their confidence level for their answer on a 5-point certainty scale. Inter-rater reliability

between scorer pairs was assessed on a lobar basis using Cohen's kappa values, first in terms of whether or not they felt the SOZs for each case included the temporal lobe. We then performed this separately for the frontal lobe, but not other regions (e.g. parietal, occipital, insula) due to progressive imbalance with fewer SOZ observations in these regions (Table S1).

The specific OPSCEA-based SOZ localization answers were then compared to the CRS to assess accuracy. Responses were deemed "overlapping" if the scorer named one or more correct areas but left out (or unnecessarily added) an additional lobe and/or region compared to the CRS. For example, if a CRS report indicated simultaneous hippocampus and lateral temporal cortex involvement in the seizure onset, a response of "hippocampus" would be overlapping whereas a fully correct response would name both regions. Accuracy was defined as the percentage of cases correctly identified (lobe, and separately for focus) out of the total number of cases. Since chance levels are progressively lower with more structures sampled, and the number of structures sampled varied from case to case, the use of standard binary measures of inter-rater reliability (e.g. Cohen's kappa) is undermined for localization accuracy. We instead assessed localization concordance: whether scorers (in pairwise comparisons to each other) were consistently correct or incorrect in identifying the CRS-defined SOZ. We also used receiver operating characteristic curves to assess whether confidence levels predicted scorer accuracy.

RESULTS

Demographic and clinical data for the 41 included patients (23F/18M) are shown in Table S1. Ages ranged from 5 to 50 years old (median 31). Their ages of epilepsy onset ranged from 1 to 47 years old, with a 1- to 32-year history of epilepsy prior to invasive monitoring. There were 13 SEEG cases (depths only), 6 subdural cases (limited to grids ± strips), and 22 hybrid cases (both). Among these, 24 were left-sided cases, 14 right-sided, and 3 bilateral. The median number of electrodes per patient for OPSCEA videos was 117 (range: 48 to 313). Median follow-up time was 1.71 years. Table S1 also shows the CRS.

Standard video frames included simultaneous views of surface and depth electrode activity, along with the corresponding raw ICEEG. Users were oriented to any depth-electrode slice views by colored trajectory lines over surface views (Figure 2D). Figure 3 shows an example of the strengths of omni-planar views in visualizing not only seizure onset but propagation, here from the temporal to frontal lobes and beyond (see Video S2). This rapid pattern clarified pre-surgical scalp EEG findings which had interpreted both temporal and frontal sources. The patient received a right anterior temporal lobectomy (no extratemporal resection) and is seizure free for >1 year.

As shown in Figure S1, the evolution of an ictal pattern in a single electrode over time can be detected and sustained using the zLL transform, despite a large dynamic shift in the peak frequency admixtures which undermines approaches using fixed bands for seizure evolution(10). Figure 4A (also see Video S3) shows an example of a seizure with a prolonged aura and semiology sequence, lasting around 8 minutes. This seizure spread

slowly across multiple lobes of the brain and the semiology evolves accordingly in Jacksonian-like fashion.

Since ICEEG transforms can provide frame rates down to the sampling rate of raw data, rapid and broad ictal network propagation can be more simply visualized. As shown in Figure 4B (also see Video S4), sudden onsets can be delineated anatomically with a higher FPSD, and the spatial distribution displayed down to the microsecond level.

Ictal-onset video renderings for 41 patients were used to assess whether scorers from various levels of expertise were able to determine the lobe, and focus (i.e. lobule, gyrus, or other sublobar structure) involved at initial seizure onset (whether unifocal or multifocal/multilobar). These OPSCEA-based determinations were compared to the CRS answers to determine accuracy (Figure 5A). The correct lobe(s) was/were accurately identified in 90.2-97.6% for overlapping responses and 73.2-82.9% for fully correct responses. When assessing only patients in whom the CRS was considered well-localized on the original ICEEG study (N=30), this rose to 90.0-100.0% and 80.0-96.7% respectively. Inter-rater reliability (Cohen's kappa values) between the scorers ranged from 0.53-0.85 regarding whether or not the SOZ included temporal lobe and from 0.36-0.72 regarding whether or not the SOZ included frontal lobe. Agreement increased to 0.60-1.0 and 0.79-1.0 respectively when including only patients with an Engel I outcome (Figure S3).

The correct focus(i) was/were accurately identified in 87.8-95.1% for overlapping responses and 56.1-63.4% for fully correct responses. When assessing only patients in whom the CRS was considered well-localized on the original ICEEG study (N=30), this rose to 90.0-93.3% and 63.3-73.3% respectively. No clear difference was observed across expertise levels though we were underpowered to assess this statistically. Interestingly, the attending epileptologist scored highest for identifying the fully correct focus(i) (63.4%, 73.3% in well-localized cases only).

Better surgical outcomes are associated with better CRS localization of seizures(23), a relation potentially mirrored in functional 3D localization(10). Therefore we split the patients according to good (Engel I) versus poor (Engel II-IV) groups(24). OPSCEA-based identifications of the (fully) correct lobe and focus were indeed better for patients with a good outcome ($p<0.001$ and $p=0.0489$ respectively, paired t-test; Figure 5B) but this did not matter for the overlapping conditions ($p>0.05$). Concordance between scorers for both correct and incorrect responses ranged from 51.2% agreement between the two residents to 80.5% agreement between the attending and fellow (Figure 5C).

Grouping responses by focus(i) localization accuracy on the 5-point certainty scale showed that, relative to incorrect responses, correct responses were associated with greater confidence by the scorers ($p=0.0377$ and $p=0.008$ for overlapping or fully correct respectively, paired t-tests; Figure 5D). As an extension, implementing this certainty scale as a predictor of correctly identifying the seizure focus with ROC curves (Figure S4) illustrated AUC's ranging from 0.57 to 0.73 (chance would be approximately 0.5 on average using random data; Table S2) for the most challenging task of identifying the fully correct focus(i).

DISCUSSION

We present a cinematic method to visualize epileptiform activity in both deep and superficial brain regions simultaneously for comprehensive and intuitive intracranial seizure localization. Our primary goal was to overcome the challenge of visualizing ictal onset and spread in deep regions (such as the hippocampus, amygdala, and insular cortex) simultaneously with cortical surface views, as opposed to previous similar cinematic approaches which reported on cortical surface views only(6,10). This is particularly important given the rising use of SEEG(3,15) where both deep and superficial sites are routinely sampled. Deep lesions, such as focal cortical dysplasias and polymicrogyria extensions, are also crucial to visualize in certain cases. Often these common seizure onset sources can only be sampled with depth electrodes, and require variable trajectories(25,26). Indeed, both between and even within institutions, depth electrode trajectories and naming patterns often lack standardization(27), complicating interpretation and inter-provider communications. Our secondary goal was to decrease the work of the user in signal processing requirements and parameter calibration.

The two main innovations are therefore 1) functional projection of depth electrode activity using omni-planar slice reconstructions in-line with probe trajectories fused to surface views, and 2) application of a normalized LL transform to accentuate diverse epileptiform features with low-supervision. We also utilize a “multi-view” approach, displaying *each* depth electrode in its own plot and multiple surface views simultaneously. This aids visualization of the SOZ as well as the appreciation of complicated spatiotemporal seizure spread patterns (Video S2) at various speeds (Videos S3, S4) which can hold additional clinical value(11,28-31).

Many biomedical imaging platforms feature omni-planar slicing and functional projection capabilities, yet to our knowledge there is no existing platform fusing these capabilities to effectively aid ICEEG SOZ visualization with the innovations above, hence our introduction of this technique and provision of example software to hopefully kindle future refinements of such methods in the field. We also include other efficient adaptations to cinematic ictal 3D projection methods, all of which are engrained in the open-source code and example cases linked with this publication.

Previous similar cinematic approaches (6,10,11) focused predominantly on beta range frequencies as an ictal surrogate, and assessed other frequency ranges only up to 50 Hz. However, pathological fast activity is an important diagnostic feature in the majority of ictal (and interictal) intracranial recordings, among other patterns(32-34), and more complex measures such as nonlinear signal analysis, connectivity, or statistical parametric mapping may provide even greater accuracy for the SOZ(12,35-37). The zLL algorithm is comparatively simple yet we have found it largely circumvents the need for frequency specification and hence has low expert supervision requirements (Figure S1; though see discussion of limitations below). Of note, the normalization step (to a pre-ictal baseline) was crucial for clarity, mitigating inter-electrode differences and unmasking dynamic changes on varying timescales (Figure 4).

The attending epileptologist achieved the highest accuracy for the specific epilepsy focus, yet only marginally above the other levels of training. Importantly however, scorers were completely blinded to clinical details (pre-operative workup, history, seizure semiology, etc), in order to isolate the efficacy of OPSCEA videos alone. Accuracy was improved for patients who had a good surgical outcome consistent with Lee et al(10), and in line with the notion that determining the SOZ more conclusively affords more definitive surgical treatment. Corroborating this, higher levels of confidence by the scorers predicted better identification of the SOZ (lobe>focus), most notably for the epilepsy fellow (Table S2). These findings suggest that OPSCEA may be useful as an adjunct tool for use in epilepsy surgery planning, particularly when coupled with increased confidence in assessment for a given case, though future prospective studies are needed.

Limitations of our method are largely inherent to ICEEG recordings themselves, including the lack of information in regions which there is no electrode coverage. While we found this method to be interpretable for those with and without formal epilepsy training (Figure 5), this technique purposely oversimplifies the data which may contain important additional details (e.g. polarity, frequency admixture, waveform morphology), and thus could pose overcertainty risks (note certainty levels for student vs. attending in Figure 5D despite accuracy results in 5A). Another limitation is that for some patients, the SOZ features a focal attenuation of activity, which would generate low LL values; however, focal attenuation could be tracked if desired by assigning alternate color schemes to *negative* shifts in zLL values. The LL transform tends to assign higher values to certain epileptiform features (particularly pathological high frequencies) than others (Figure S1A-B)(18). This could cause a relative bias between channels depending on the dominant frequencies at seizure onset, or within the same channel as the ictal pattern evolves in mixture of frequencies over time. This problem is also inherent to, and potentially more problematic for, power-based heatmaps as described previously (10) and as illustrated in Figure S1. Further work is required to improve the sensitivity, specificity, and application of such epileptiform activity visualization approaches(12,35-37). Meanwhile, providing multiple adjustable visualization options to the provider seems an optimal current solution (e.g. flexible transform window durations and FPSD, and using LL or specific power bands if desired), similar to adjusting filters and other signal parameters in current clinical trace-based ICEEG reading.

An additional limitation is the independent fashion in which scorers interpreted the videos compared to the trace-based CRS which incorporated additional clinical information (clinical history, other imaging studies, semiology, etc.). This was by design to help discern whether OPSCEA could provide meaningful clinical information in isolation (considering other functional diagnostic studies like scalp EEG source localization, PET, and SPECT), but future work will ideally assess whether OPSCEA or similar technologies add meaningful diagnostic value in prospective clinical decision-making that includes all available diagnostic tests(38).

As intracranial recordings rise in complexity and density(2), dynamic functional projection techniques will be increasingly useful to understand seizure onset and spread patterns, and perhaps even shed more light on the associations between anatomy, neurophysiology, and semiology on linked video(6). Such methods also provide an intuitive visualization of

subsequent spatial spread patterns of seizures (Figure 4), which can further inform resective surgical planning and/or placement of electrodes for responsive neurostimulation(39). Lastly, cinematic visualization helps illustrate of the speed of the ictal wavefront across deep and superficial structures, and the spatial extent of regional ictal onsets, predictive factors for surgical outcome(11,28-31). This preliminary validation study is encouraging for the use of omni-planar ICEEG seizure visualization as an adjunct for ICEEG interpretation and surgical planning, and as a communication tool among health providers and trainees at all levels.

Supplementary Material

Refer to Web version on PubMed Central for supplementary material.

Acknowledgments:

We thank John Andrews, Sharon Chiang, and Joline Fan for critical input. This work was supported by NINDS grants R25NS070680 and K23NS110920 awarded to Jon Kleen, and R01-DC012379, R00-NS065120 awarded to Edward Chang.

REFERENCES

1. Baud MO, Perneger T, Rácz A, Pensel MC, Elger C, Rydenhag B, et al. European trends in epilepsy surgery. Neurology. 2018 10;91(2):e96–106. [PubMed: 29898967]
2. Chang EF. Towards large-scale, human-based, mesoscopic neurotechnologies. Neuron. 2015 4 8;86(1):68–78. [PubMed: 25856487]
3. Cardinale F, Casaceli G, Raneri F, Miller J, Lo Russo G. Implantation of Stereoelectroencephalography Electrodes: A Systematic Review. J Clin Neurophysiol Off Publ Am Electroencephalogr Soc. 2016 12;33(6):490–502.
4. Hamilton LS, Chang DL, Lee MB, Chang EF. Semi-automated Anatomical Labeling and Inter-subject Warping of High-Density Intracranial Recording Electrodes in Electrocorticography. Front Neuroinformatics. 2017;11:62.
5. Fischl B. FreeSurfer. NeuroImage. 2012 8 15;62(2):774–81. [PubMed: 22248573]
6. Youngblood MW, Han X, Farooque P, Jhun S, Bai X, Yoo JY, et al. Intracranial EEG surface renderings: new insights into normal and abnormal brain function. Neurosci Rev J Bringing Neurobiol Neurol Psychiatry. 2013 6;19(3):238–47.
7. Duez L, Tankisi H, Hansen PO, Sidenius P, Sabers A, Pinborg LH, et al. Electromagnetic source imaging in presurgical workup of patients with epilepsy: A prospective study. Neurology. 2019 2 5;92(6):e576–86. [PubMed: 30610090]
8. Englot DJ, Yang L, Hamid H, Danielson N, Bai X, Marfeo A, et al. Impaired consciousness in temporal lobe seizures: role of cortical slow activity. Brain J Neurol. 2010 12;133(Pt 12):3764–77.
9. Baud MO, Kleen JK, Anumanchipalli GK, Hamilton LS, Tan Y-L, Knowlton R, et al. Unsupervised Learning of Spatiotemporal Interictal Discharges in Focal Epilepsy. Neurosurgery. 2017 10 10;
10. Lee HW, Youngblood MW, Farooque P, Han X, Jhun S, Chen WC, et al. Seizure localization using three-dimensional surface projections of intracranial EEG power. NeuroImage. 2013 12;83:616–26. [PubMed: 23850575]
11. Andrews JP, Gummadavelli A, Farooque P, Bonito J, Arencibia C, Blumenfeld H, et al. Association of Seizure Spread With Surgical Failure in Epilepsy. JAMA Neurol. 2018 12 3;
12. Ayoubian L, Tadel F, David O. Epileptogenicity Mapping: A Quantitative Approach to Identify the Seizure Onset. Neurosurg Clin N Am. 2020 7 1;31(3):449–57. [PubMed: 32475492]
13. Tadel F, Baillet S, Mosher JC, Pantazis D, Leahy RM. Brainstorm: A User-Friendly Application for MEG/EEG Analysis. Comput Intell Neurosci [Internet]. 2011 [cited 2020 Dec 2];2011. Available from: https://www.ncbi.nlm.nih.gov/pmc/articles/PMC3090754/

14. Oostenveld R, Fries P, Maris E, Schoffelen J-M. FieldTrip: Open Source Software for Advanced Analysis of MEG, EEG, and Invasive Electrophysiological Data. Comput Intell Neurosci [Internet]. 2011 [cited 2020 Dec 2];2011. Available from: https://www.ncbi.nlm.nih.gov/pmc/articles/PMC3021840/
15. Cardinale F, Cossu M, Castana L, Casaceli G, Schiariti MP, Miserocchi A, et al. Stereoelectroencephalography: surgical methodology, safety, and stereotactic application accuracy in 500 procedures. Neurosurgery. 2013 3;72(3):353–66; discussion 366. [PubMed: 23168681]
16. Esteller R, Echauz J, Tcheng T, Litt B, Pless B. Line length: an efficient feature for seizure onset detection. In: 2001 Conference Proceedings of the 23rd Annual International Conference of the IEEE Engineering in Medicine and Biology Society [Internet]. Istanbul, Turkey: IEEE; 2001 [cited 2019 Jan 20]. p. 1707–10. Available from: http://ieeexplore.ieee.org/document/1020545/
17. Bergstrom RA, Choi JH, Manduca A, Shin H-S, Worrell GA, Howe CL. Automated identification of multiple seizure-related and interictal epileptiform event types in the EEG of mice. Sci Rep. 2013;3:1483. [PubMed: 23514826]
18. Duckrow RB, Tcheng TK. Daily variation in an intracranial EEG feature in humans detected by a responsive neurostimulator system. Epilepsia. 2007 8;48(8):1614–20. [PubMed: 17442001]
19. Liu Y, Coon WG, de Pesters A, Brunner P, Schalk G. The effects of spatial filtering and artifacts on electrocorticographic signals. J Neural Eng. 2015 10;12(5):056008. [PubMed: 26268446]
20. Einevoll GT, Kayser C, Logothetis NK, Panzeri S. Modelling and analysis of local field potentials for studying the function of cortical circuits. Nat Rev Neurosci. 2013 11;14(11):770–85. [PubMed: 24135696]
21. Bottan JS, Rubino PA, Lau JC, MacDougall KW, Parrent AG, Burneo JG, et al. Robot-Assisted Insular Depth Electrode Implantation Through Oblique Trajectories: 3-Dimensional Anatomical Nuances, Technique, Accuracy, and Safety. Oper Neurosurg Hagerstown Md. 2020 3 1;18(3):278–83.
22. Vakharia VN, Sparks R, Rodionov R, Vos SB, Dorfer C, Miller J, et al. Computer-assisted planning for the insertion of stereoelectroencephalography electrodes for the investigation of drug-resistant focal epilepsy: an external validation study. J Neurosurg. 2018 4 1;1–10.
23. Krucoff MO, Chan AY, Harward SC, Rahimpour S, Rolston JD, Muh C, et al. Rates and predictors of success and failure in repeat epilepsy surgery: A meta-analysis and systematic review. Epilepsia. 2017;58(12):2133–42. [PubMed: 28994113]
24. Engel J Update on surgical treatment of the epilepsies: Summary of The Second International Palm Desert Conference on the Surgical Treatment of the Epilepsies (1992). Neurology. 1993 8 1;43(8):1612–1612. [PubMed: 8102482]
25. Maillard LG, Tassi L, Bartolomei F, Catenoix H, Dubeau F, Szurhaj W, et al. Stereoelectroencephalography and surgical outcome in polymicrogyria-related epilepsy: A multicentric study. Ann Neurol. 2017 11;82(5):781–94. [PubMed: 29059488]
26. Perucca P, Dubeau F, Gotman J. Intracranial electroencephalographic seizure-onset patterns: effect of underlying pathology. Brain J Neurol. 2014 1;137(Pt 1):183–96.
27. Bulacio JC, Chauvel P, McGonigal A. Stereoelectroencephalography: Interpretation. J Clin Neurophysiol Off Publ Am Electroencephalogr Soc. 2016 12;33(6):503–10.
28. Ma BB, Fields MC, Knowlton RC, Chang EF, Szaflarski JP, Marcuse LV, et al. Responsive neurostimulation for regional neocortical epilepsy. Epilepsia. 2020 1;61(1):96–106. [PubMed: 31828780]
29. Smith EH, Liou J, Davis TS, Merricks EM, Kellis SS, Weiss SA, et al. The ictal wavefront is the spatiotemporal source of discharges during spontaneous human seizures. Nat Commun. 2016 3 29;7:11098. [PubMed: 27020798]
30. Liou J-Y, Smith EH, Bateman LM, McKhann GM, Goodman RR, Greger B, et al. Multivariate regression methods for estimating velocity of ictal discharges from human microelectrode recordings. J Neural Eng. 2017 8;14(4):044001. [PubMed: 28332484]
31. Andrews JP, Ammanuel S, Kleen J, Khambhati AN, Knowlton R, Chang EF. Early seizure spread and epilepsy surgery: A systematic review. Epilepsia. 2020;61(10):2163–72. [PubMed: 32944952]

32. Ayoubian L, T F, D O. Epileptogenicity Mapping: A Quantitative Approach to Identify the Seizure Onset [Internet]. Vol. 31, Neurosurgery clinics of North America. Neurosurg Clin N Am; 2020 [cited 2020 Dec 2]. Available from: https://pubmed.ncbi.nlm.nih.gov/32475492/

33. Lagarde S, Buzori S, Trebuchon A, Carron R, Scavarda D, Milh M, et al. The repertoire of seizure onset patterns in human focal epilepsies: Determinants and prognostic values. Epilepsia. 2019 1;60(1):85–95. [PubMed: 30426477]

34. Frauscher B, Bartolomei F, Kobayashi K, Cimbalnik J, van 't Klooster MA, Rampp S, et al. High-frequency oscillations: The state of clinical research. Epilepsia. 2017;58(8):1316–29. [PubMed: 28666056]

35. Bartolomei F, Lagarde S, Wendling F, McGonigal A, Jirsa V, Guye M, et al. Defining epileptogenic networks: Contribution of SEEG and signal analysis. Epilepsia. 2017;58(7):1131–47. [PubMed: 28543030]

36. Grinenko O, Li J, Mosher JC, Wang IZ, Bulacio JC, Gonzalez-Martinez J, et al. A fingerprint of the epileptogenic zone in human epilepsies. Brain. 2018 1;141(1):117. [PubMed: 29253102]

37. Woolfe M, Prime D, Gillinder L, Rowlands D, O'keefe S, Dionisio S. Automatic detection of the epileptogenic zone: An application of the fingerprint of epilepsy. J Neurosci Methods. 2019 9 1;325:108347. [PubMed: 31330159]

38. Knowlton RC, Elgavish R, Howell J, Blount J, Burneo JG, Faught E, et al. Magnetic source imaging versus intracranial electroencephalogram in epilepsy surgery: a prospective study. Ann Neurol. 2006 5;59(5):835–42. [PubMed: 16634031]

39. Ma BB, Rao VR. Responsive neurostimulation: Candidates and considerations. Epilepsy Behav EB. 2018;88:388–95.

Key points:

- Cinematic heatmaps on 3D brain reconstructions illustrate seizure activity *in situ*
- Oblique slices along depth electrodes enable functional visualization on deep anatomy
- Projecting a colorized line-length transform emphasizes seizure activity with low user effort
- The combined approach was clinically validated in comparison to standard trace-based localization

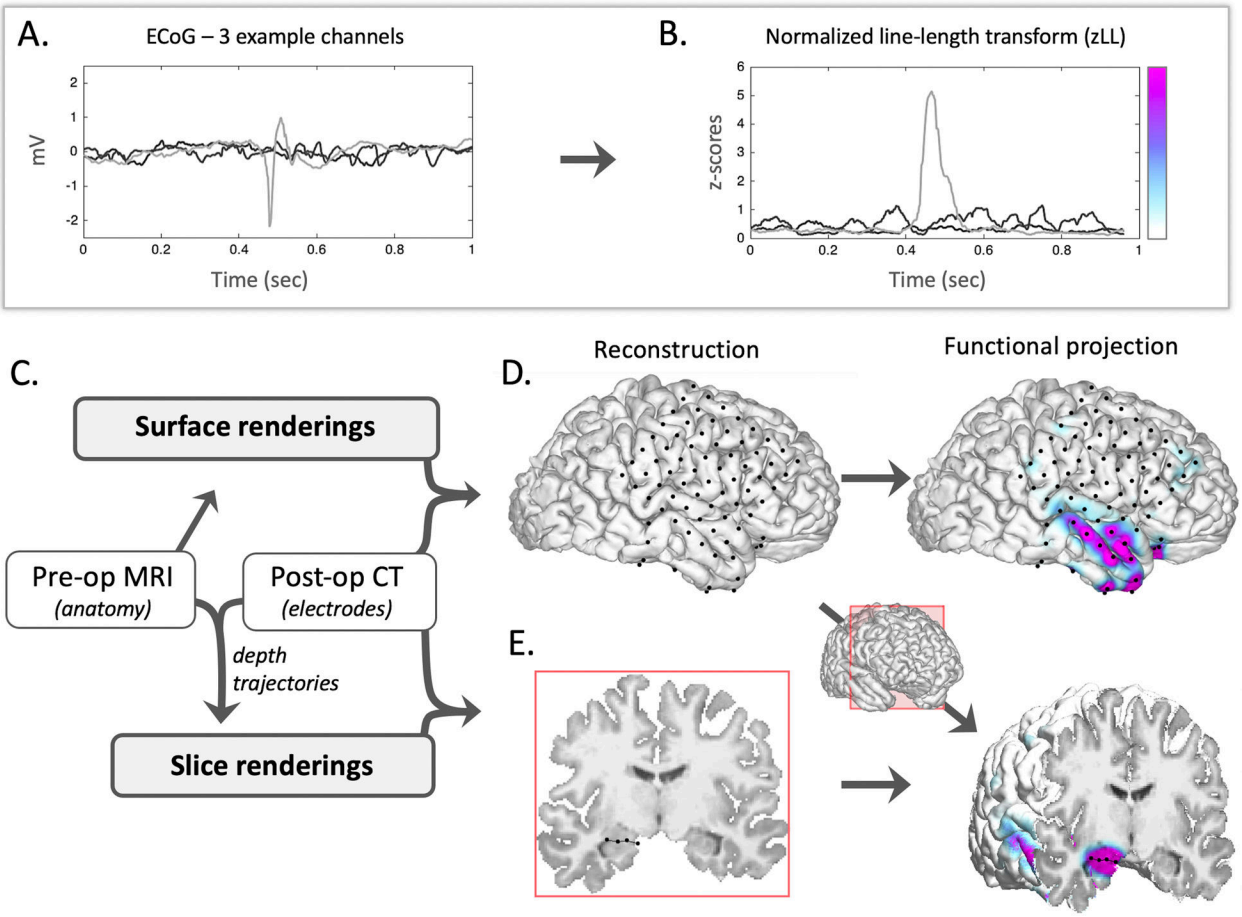

Figure 1.

Omni-planar and surface casting of epileptiform activity (OPSCEA) method and workflow. **A**. Three continuous traces of ICEEG, one containing an epileptiform spike (light grey). **B**. Line-length sliding window (point-by-point) transform of data in A using a 250 ms example transform window (normalized to an earlier baseline segment). The y-axis (zLL) is aligned to a multi-color scale for functional projection which desaturates approaching zero. **C**. Imaging pipeline converting the pre-operative MRI into a digital mesh rotatable in 3D along with co-registered electrode contact sites projected into the same space (see D). The pipeline then produces omni-planar renderings using the depth-electrode coordinates to automatically generate a slice for each depth electrode from the T1-weighted volume (see E). **D**. Digital surface reconstruction with co-registered electrodes (black dots). Functional activity, in our method using the zLL transform, is projected onto the surface (right panel) using a Gaussian-weighted recoloring based on signal intensity and distance from the electrode(6,10). **E**. The zLL transform is projected onto omni-planar slices in a similar manner, and the surface (inset with slice cross-section) and slice views are merged and plotted together for an intuitive view of both deep and superficial epileptiform activity (OPSCEA). In the example patient depicted in D and E (Patient 1), a seizure began in the mesial temporal structures (4-contact depth), and subsequently spread to the lateral temporal cortex depicted in this partial frame.

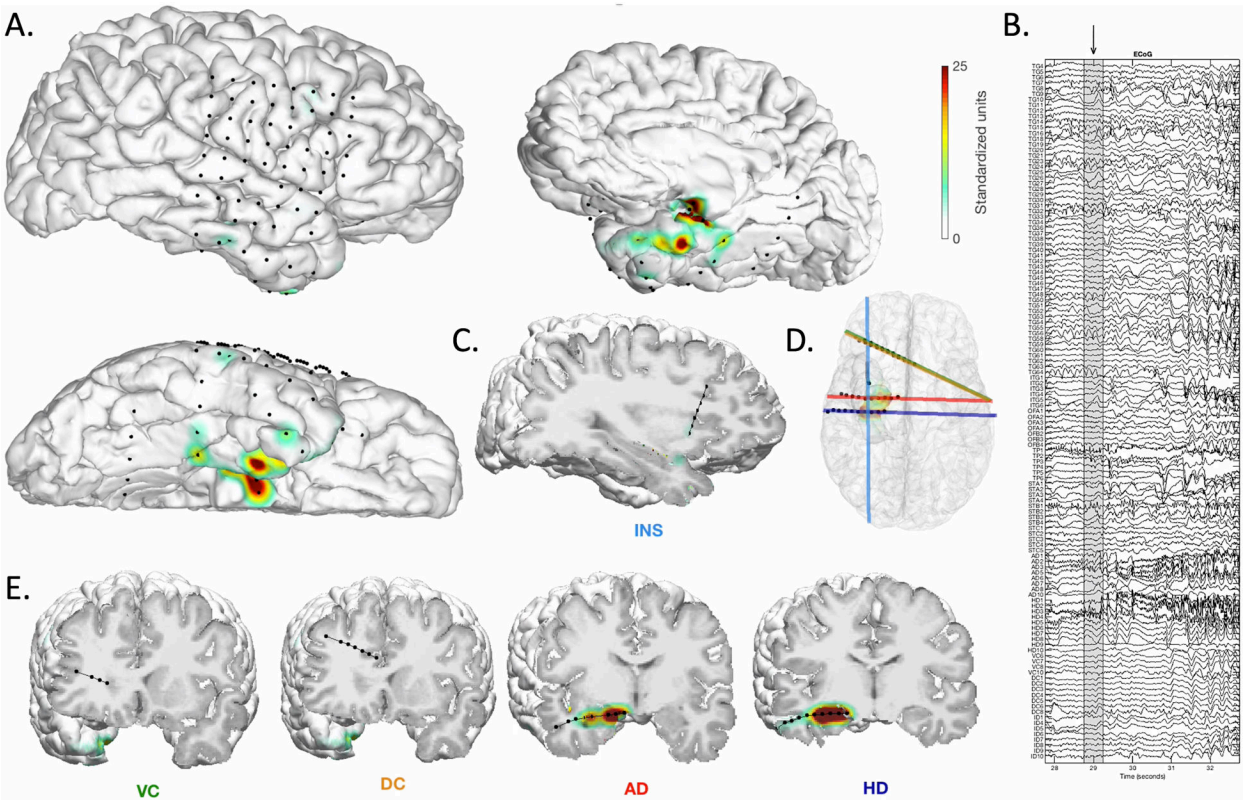

Figure 2.

Example frame of standard OPSCEA display with hybrid combination of subdural grids, strips, and five depth probes. **A**. Three-dimensional lateral view of right hemisphere surface, with rotated inferior (bottom panel) and antero-infero-medial (right panel) views to enable visualization of co-registered surface electrode contacts (black dots=channels; channels with low or artifactual signal omitted). The zLL values for each electrode are projected onto these surfaces (Gaussian drop-off according to the color axis at far right), illustrating focal mesial temporal seizure activity (see corresponding Video S1). **B**. ICEEG recording, with channels in order of original recording montage, and grey shaded box ("transform window") highlighting the data corresponding to the activity projected simultaneously in the other panels. During blinded scoring channel order was randomized and labels hidden. **C**. Near-parasagittal omni-planar MRI slice view along the insula depth (INS). **D**. Semi-transparent ("glass") view of the inferior surface of both hemispheres with black depth electrode contacts, and colored lines marking the oblique slice levels for corresponding omni-planar views of each individual depth probe, shown in C (blue line). Grid and strip electrodes are hidden for clarity, and the hippocampus and amygdala surfaces are also included for perspective. **E**. Near-coronal omni-planar MRI slice views of remaining individual depth electrodes targeting the ventral cingulate (VC), dorsal cingulate (DC), amygdala (AD), and hippocampus (HD). Colored labels correspond to trajectory lines in D. The zLL values are projected onto slice surfaces, illustrating focal seizure activity around contacts in the hippocampus and amygdala.

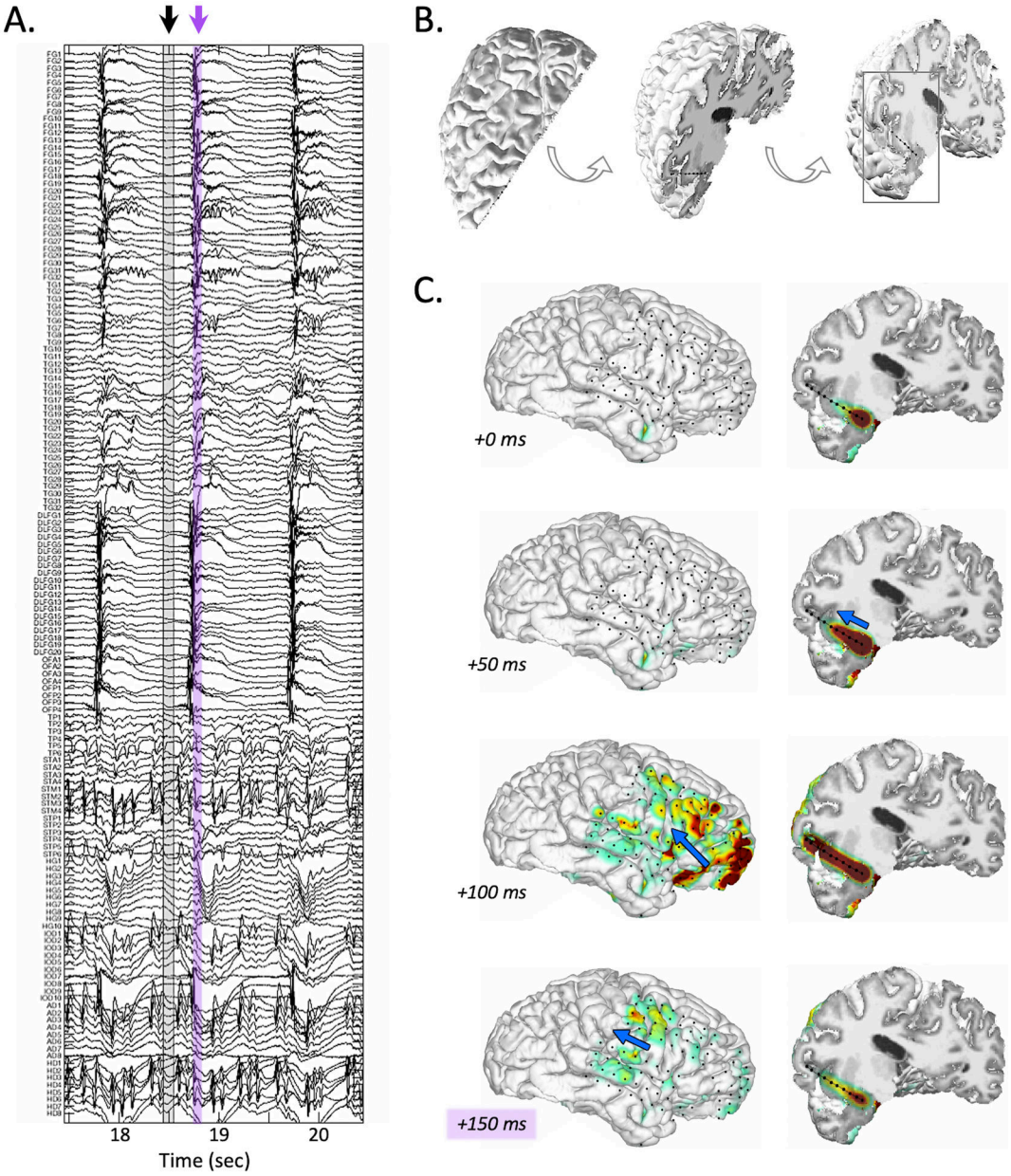

Figure 3.

Example of seizure spread across both deep and superficial sites. **A**. ICEEG traces showing an ongoing focal mesial temporal seizure (Patient 29; see corresponding Video S2), yet with intermittent broad discharges (~1 Hz) raising concern for a widespread network throughout numerous temporal, frontal, and parietal sites (50 ms transform window in grey corresponds to top panel in C, purple window corresponds to bottom panel). **B**. Rotating views from superior (left panel) to anterior (right) of an omni-planar slice+surface composite reconstruction for the depth probe labeled “IOD”. From superficial to deep this probe samples the frontal cortex, anterior insula, and piriform cortex (frontal-temporal transition). **C**. Time-lapse of lateral surface and omni-planar IOD depth views every 50ms after the grey window in A. The discharges were not broadly synchronous, originating instead from the

focal mesial temporal seizure and rapidly propagating (small blue arrows) through cortical structures along the IOD (mesial temporal to frontal) and then posteriorly (frontal to parietal).

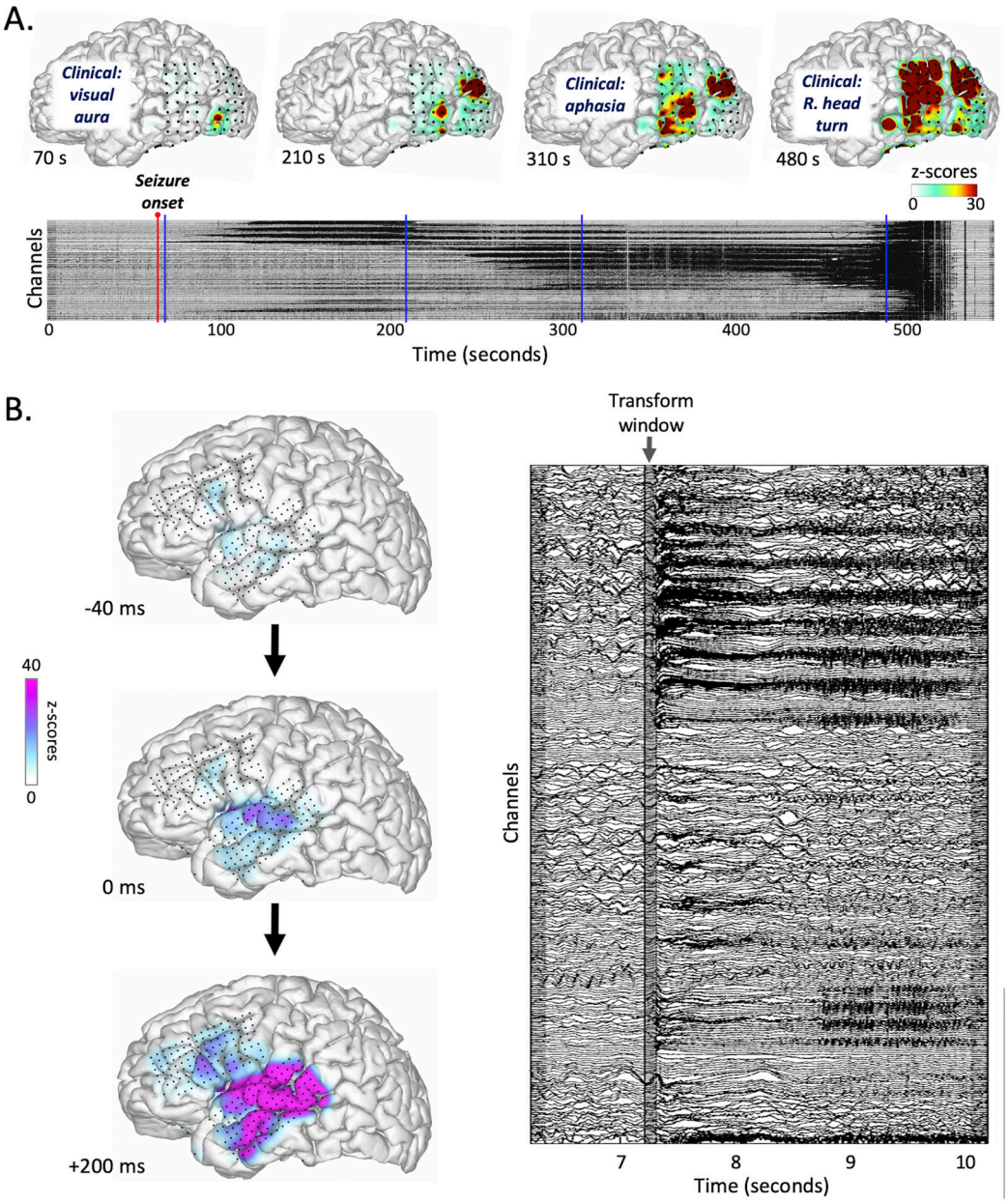

Figure 4.

Tracking extreme seizure spread timescales. **A**. Slowly spreading seizure example (nearly 8 minutes long; Patient 20; see corresponding Video S3) with selected frame examples to highlight the unique spatial migrations of ictal activity in a given patient. The corresponding ICEEG is shown in the center, with a red line at seizure onset and blue vertical lines corresponding to the consecutive OPSCEA views shown and labeled along with time (seconds) in gray. The patient's reported clinical symptoms and semiology at distinct timepoints are also labeled in blue on the corresponding surfaces. This seizure began electrographically at around 65 seconds into this file, in the temporo-occipital junction. Seconds later, the patient described his typical visual aura in the right-side visual field. The ictal wavefront first spread superiorly followed by anterior spread to the temporal lobe

synchronous with receptive aphasia, then suprasylvian spread with speech arrest, then a right-side head turn, and finally a bilateral tonic-clonic seizure. **B**. Rapidly spreading seizure example (Patient 10; see corresponding Video S4) showing traces recorded on high-density grids (4mm spacing) in right panel along with corresponding lateral surface views for three timepoints relative to the 50ms gray transform window position on the traces. This "explosive" onset includes rapid propagation through temporal and frontal lobes within hundreds of milliseconds, yet using a 150 FPSD for OPSCEA visualization, the core onset region was evident in the posterior superior temporal gyrus.

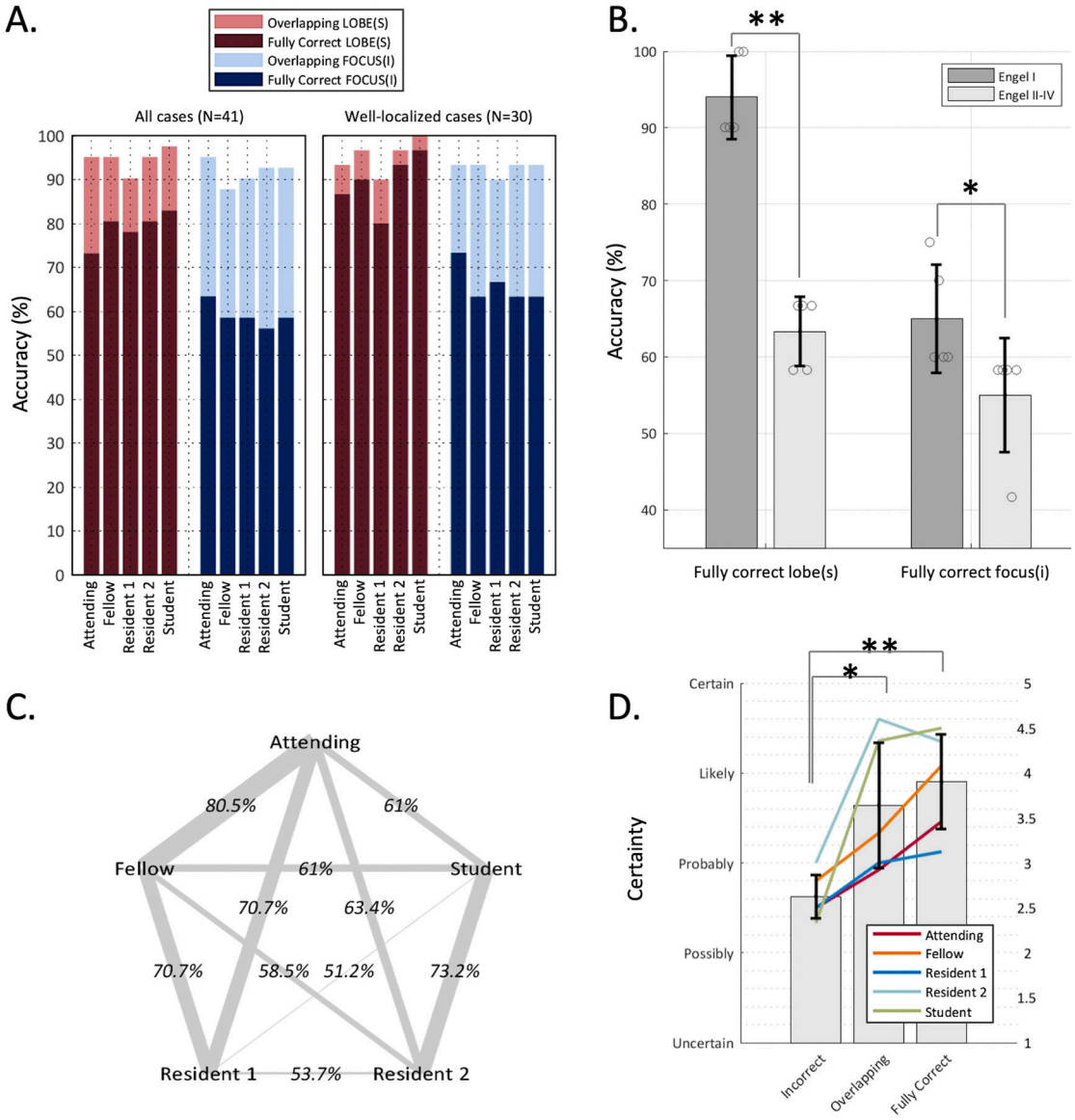

Figure 5.

OPSCEA SOZ-localization relative to original clinical decision. **A**. Accuracy of scorers across multiple levels of expertise (x-axis) is shown for OPSCEA-based SOZ-localization relative to the CRS, for full or overlapping identification of the correct lobe(s) or focus(i) (including uni-focal and multi-focal onsets). **B**. Accuracy across the conditions in A as a function of outcome as measured by Engel score (bars, standard deviation of the mean across scorers). Scorers had greater accuracy identifying the correct lobe, and borderline for focus, in patients with a better outcome (**$p<0.001$ and *$p=0.0489$ respectively, paired t-test). **C**. Concordance between scorers as measured by agreement rate for correct and incorrect responses. Highest concordance was observed between the Attending and Fellow levels. **D**. Confidence level in responses as measured by a 5-point certainty scale, averaged within each scorer (lines) and grouped by response accuracy for overlapping or fully correct focus (bars, standard deviation of the mean across scorers). Relative to incorrect responses,

scorers expressed greater confidence for overlapping and fully correct responses (*p=0.0377 and **p=0.0077 respectively, paired t-test).

Table 1.

ICEEG recording factors varying between patients.

Recording components

- Varying types: penetrating depth electrodes, surface (subdural) grids or strips
- Number of contacts per component (e.g. 4- vs. 10-contact depth, 16- vs. 64-contact grid)
- Sheer number and combination of components
- Variable spacing:
  - Inter-electrode differences (depend on manufacturer and model, e.g. 5mm, 10mm)
  - Distance of one component from another (complicated further if a strip or grid migrates)
- Orientation, for example:
  - Which corner of the grid is contact #1?
  - Which orthogonal edge is the first row?
  - For a strip positioned anterior-to-posterior, are the contacts oriented #1-to-6 or vice-versa?

Patient-specific anatomy

- Laterality of implantation: left, right, or bilateral
- Individual anatomy: distinct curve of a gyrus, depth of a sulcus
- Lesions or prior resection sites

ICEEG data review

- Montage:
  - Order of components on screen
  - Order within a component on screen
- Component labeling, for example:
  - PG: *P*arietal vs. *P*osterior *G*rid?
  - AD: *A*mygdala-targeted *D*epth vs. *A*nterior-most of multiple frontal *D*epths?
  - Anatomic vs. target: Should one use HDMTG or HD for a hippocampal depth inserted in middle temporal gyrus?